Available online at www.sciencedirect.com
ScienceDirect
Journal of Nuclear Materials 375 (2008) 263–269
journal of nuclear materials
www.elsevier.com/locate/jnucmat

# Thermochemical degradation of limestone aggregate concrete on exposure to sodium fire

M. Premila [a,*], K. Sivasubramanian [b], G. Amarendra [a], C.S. Sundar [a]

[a] Materials Science Division, Indira Gandhi Centre for Atomic Research, Kalpakkam 603 102, India
[b] Safety Engineering Division, Indira Gandhi Centre for Atomic Research, Kalpakkam 603 102, India

Received 14 June 2007

**Abstract**

Limestone aggregate concrete blocks were subjected to sodium fire conforming to a realistic scenario in order to qualify them as protective sacrificial layers over structural concrete flooring in liquid metal-cooled fast breeder reactors. Mid infrared absorption measurements were carried out on these sodium fire-exposed samples as a function of depth from the affected surface. Definite signatures of thermochemical degradation indicating dehydration and structural modification of the limestone concrete have been obtained. Control runs were carried out to delineate the thermal effects of sodium fires from that of the chemical interaction effects. Measurements on limestone aggregate samples treated with fused NaOH provided direct evidence of the exact mechanism of the sodium attack on concrete. The observed degradation effects were correlated to the mechanical strength of the concrete blocks and to the intensity of the sodium fire experienced.


## 1. Introduction

The use of alkali metal sodium coolant in fast breeder reactors (FBRs) requires special consideration of its chemical reactivity and related safety problems in case of accidental sodium spillage. It is well known that when hot liquid sodium comes in contact with structural concrete, an interaction takes place due to both the thermal loading of the concrete and the chemical reactivity of the liquid metal with the constituents of concrete [1,2]. The most important consequences of the sodium-concrete interactions are the release of free and bound water from concrete leading to hydrogen generation that would ultimately result in loading of the containment chamber due to pressure build up, in addition to degrading the mechanical strength of the structural concrete itself [1–3]. In spite of adequate safety measures taken during the design, fabrication and operation stages of liquid metal-cooled fast breeder reactors, there is still a possibility of leakage of hot liquid sodium from primary and secondary heat transport circuits of the reactor during operation. Especially, so in the air filled enclosures of the steam generator building, where the sodium spills not only react with air causing fires but also result in the interaction of hot sodium (550 °C) with the structural concrete flooring. Among the several measures taken to limit/eliminate such interactions [4–6], the use of sacrificial mortar layers on structural concrete flooring is being preferred [7,8] due to key factors like economy, ease of castability, frequent demolition of affected concrete in the event of a sodium fire, disposability of debris and easy recasting. Among the several types of concrete, limestone aggregate concrete is said to be more resistant to sodium fires due to its high reaction temperature threshold [1,9]. In this context, it becomes necessary to further qualify and explore the possibility of using limestone aggregate concrete as protective sacrificial layers over structural concrete flooring. In view of this, limestone concrete test blocks with a central cavity were cast and subjected to sodium fires simulating a typical hot sodium leak in the

* Corresponding author.
*E-mail address:* premila@igcar.gov.in (M. Premila).

0022-3115/$ - see front matter © 2008 Elsevier B.V. All rights reserved.
doi:10.1016/j.jnucmat.2008.01.005

non-inerted atmospheres of breeder reactors [10]. Samples were collected at different depths from the affected surface in order to generate a depth profile of the degradative effects. While the extent of mechanical damage to the blocks were estimated using rebound hammer tests, ultrasonic pulse velocity measurements, weight loss measurements and compressive strength testing, the extent of chemical damage was estimated by generating the depth profile of sodium monoxide concentration for each block [10]. Although sodium-concrete interactions have been investigated using several other techniques [1–3,10], in the present work we have used infrared spectroscopy for the first time in an attempt to obtain direct evidence of the thermochemical degradation in sodium fire-exposed limestone concrete samples and hence generate a depth profile of the degradative effects. It is well known that the key mechanism for the setting and hardening of cement involves hydration of the anhydrous silicate and aluminate phases present in them to form the corresponding hydrates [11,12]. Hence, it immediately becomes important to follow the hydration kinetics to understand the extent of setting/degradation in these materials. Since infrared spectroscopy is a powerful tool to probe the state of hydration water [11] in addition to providing useful information of the associated chemical changes, it was of interest to use this technique to estimate the extent of damage to the sodium fire-exposed limestone concrete samples. Here we report on the mid infrared absorption measurements carried out on several samples from two different blocks whose central cavity has been exposed to sodium fires, as a function of depth from the affected surface. Apart from the changes seen in the features corresponding to vibration modes of water, splitting of two of the pristine modes of limestone along with the emergence of a new mode clearly indicates a structural modification of the limestone aggregates. Measurements were also carried out on heat-treated reference samples to delineate the thermal effects of the sodium fire from that of the chemical interaction effects of sodium with concrete. In an effort to understand the mechanism of the chemical attack of sodium on limestone concrete, measurements were also done on reference samples treated with hot fused NaOH.

## 2. Experiment

Limestone concrete test blocks – Block I and II each of dimension $600 \times 600 \times 300\ mm^3$ with a cavity size of $300 \times 300 \times 150\ mm^3$ which is centrally located on the top were cast (Fig. 1) along with reference blocks of composition 48 wt% limestone as coarse aggregate, 32 wt% limestone as fine aggregate, 13 wt% of 53 grade ordinary Portland cement and 7 wt% of potable water. Details of the experimental set up and sodium transfer procedure are given in an earlier report [10]. Thermocouples were embedded at select positions in the concrete blocks in order to monitor the temperature profile of the blocks during sodium exposures. Around 12 kg of hot liquid sodium

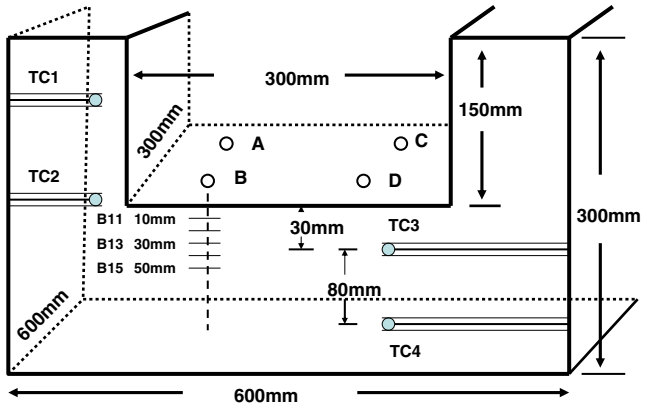


Fig. 1. Schematic of the dimensional details of test concrete block. TC1, TC2, TC3 and TC4 indicate the positions of the thermocouples. Note the location of the four positions A, B, C and D on the cavity surface from which samples were removed at different depths. B11, B12, B13, B14 and B15 correspond to samples removed at depths 10, 20, 30, 40 and 50 mm, respectively from location 'B' of block I. The same nomenclature holds good for all other samples from different locations.

was transferred on to the central cavity of the concrete blocks and allowed to be in contact with the concrete surface for a typical period of 30 minutes [10]. After the exposure, samples were drilled out from four different locations on the surface marked A, B, C and D for various depths 10–50 mm from the surface of each block. Room temperature FTIR absorption measurements were carried out on these sodium-exposed powder samples in KBr matrix using a Bomem DA8 spectrometer operating with a resolution of $4\ cm^{-1}$ in the mid infrared range using a combination of KBr beamsplitter and a liquid nitrogen cooled MCT detector. Samples were labeled as B11, A12 ... – where for instance B11 would mean a sample from position B on the surface from block I and from depth of 0–10 mm. Spectra of the samples removed from concrete blocks that were unexposed to sodium were also recorded that served as a reference. Further, in order to delineate the thermal effects from the chemical effects, reference samples were heat-treated at several temperatures 100–800 °C for a period of 30 min and their spectra recorded. Samples were also heat-treated with fused NaOH at 450 °C for 30 min in an attempt to understand the exact mechanism of attack of sodium on concrete.

## 3. Results and discussion

Fig. 2(a) shows the room temperature mid infrared spectrum (400–4000 $cm^{-1}$) of the limestone aggregate reference concrete along with the sodium exposed samples as a function of depth for Block I position 'B'. The spectrum of the reference sample revealed phonon features corresponding to the major constituent – limestone ($CaCO_3$) in the sample. Further, one can also infer that the limestone in the sample is principally in the form of calcite [13,14] as identified by its main absorption features at 1425($\nu_3$), 876($\nu_2$) and 712 $cm^{-1}$($\nu_4$). While $\nu_2$ and $\nu_3$ represent the out-of-

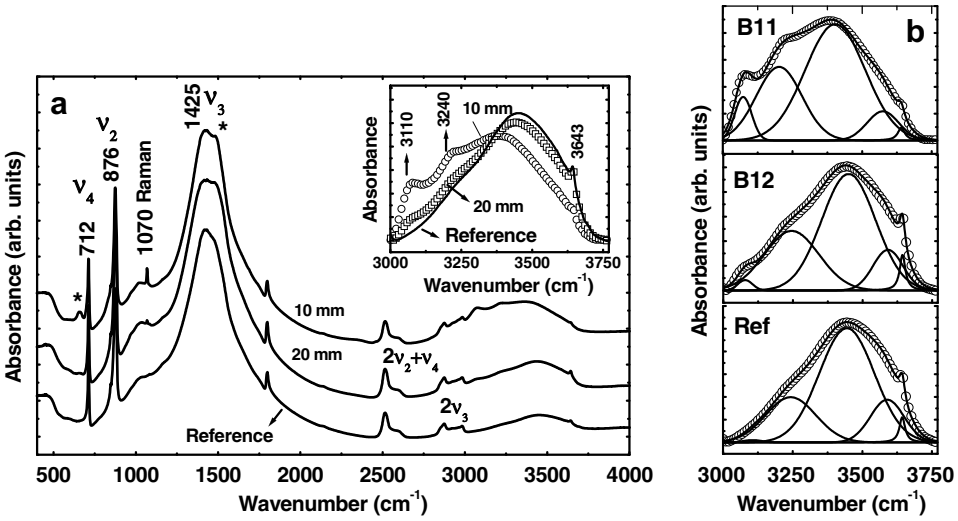


Fig. 2. (a) Room temperature spectra of unexposed reference limestone concrete sample along with sodium exposed sample B11 (10 mm) and B12 (20 mm) from the sodium-concrete interface. * indicates the new modes arising due to splitting of the pristine modes. Inset shows the area normalised absorption features of water – notice the dramatic downshift associated with significant increase in the low frequency components for samples close to the interface. Right panel (b) shows the fit in the same region (3000–3770 $cm^{-1}$).

plane bending and the asymmetric stretching of the carbonate group, respectively, $v_4$ represents the in-plane bending of the carbonate group. The features at 1788, 2512, 2872 and 2981 $cm^{-1}$ represent combination modes, while the absorption feature centered round 3500 $cm^{-1}$ is attributed to stretching mode of bound water in concrete. In particular the sharp feature at 3643 $cm^{-1}$ riding on the broad water background is said to arise due to the O–H stretching of $Ca(OH)_2$ – the major hydration product of Portland cement [11,12]. The extent of setting of cement can be followed by estimating the area under this peak at 3643 $cm^{-1}$ [11]. It is clearly evident that the spectrum of the sodium-exposed sample B11 removed from near the affected surface (10 mm from surface) shows appreciable changes as compared to that of the reference sample. The stretching modes of water in B11 reveal a significant softening associated with a dramatic increase in the intensity of the low frequency components as compared to that of the reference sample (see inset Fig. 2(a)). The intensity of the 3643 $cm^{-1}$ peak corresponding to O–H stretching mode of $Ca(OH)_2$ is also seen to significantly decrease in B11. In addition, one can also clearly see the appearance of a new phonon mode at 1070 $cm^{-1}$ and a splitting of the doubly degenerate $v_3$ and $v_4$ modes. The above signatures are indicative of a thermochemical degradation of concrete arising due to the attack of hot liquid sodium and have been understood/ rationalized as follows.

The region between 3000–3770 $cm^{-1}$ in the spectrum is dominated by the spectroscopic features of liquid water. It is well documented that the broad absorption feature due to water can be de-convoluted into four fundamental O-H stretching modes [15]. The two low frequency modes at 3110 $cm^{-1}$ and 3240 $cm^{-1}$ have been assigned to the hydrogen-bonded components, while the high frequency modes at 3440 and 3580 $cm^{-1}$ are attributed to the non hydrogen-bonded components in liquid water [15]. A dramatic increase in the intensity of the low frequency hydrogen-bonded components at 3110 and 3240 $cm^{-1}$, associated with a correlated decrease in the high frequency non hydrogen-bonded components in B11 as compared to the reference is clearly brought out in the inset of Fig. 2(a). In order to gain further insight into the exact variation of the line shape parameters, this region of the spectrum has been fitted to a sum of four/three Gaussians in addition to a Lorentzian for the sharp feature due to $Ca(OH)_2$ (Fig. 2(b)) and the variation in line shape parameters have been extracted. Fig. 3 shows the variation of the stretching mode frequencies of water as a function of depth from the affected surface for block I and block II. It is clear from the figure that these modes exhibit a dramatic softening as compared to the reference peak frequencies for depths up to 30 mm from the sodium-concrete interface in block I, while the changes are much less pronounced for block II. Note that the reference values are plotted at a depth of 100 mm for comparison. As has been earlier mentioned the role of concrete is twofold: that of a heat sink, which results in the release of both free and bound water from the concrete and a reservoir of solid constituents available for chemical reactions. Hence, all the above signatures pertaining to degradation in the limestone aggregate concrete are in fact a combined effect resulting from the thermochemical attack of hot sodium with concrete. At this juncture it becomes interesting and important to delineate the thermal effects on the concrete due to the sodium fire from that of the chemical interaction effects.

### 3.1. Heat treatment of reference concrete

Reference samples were heat-treated at several temperatures ranging from 100 to 800 °C for 30 min each, to look

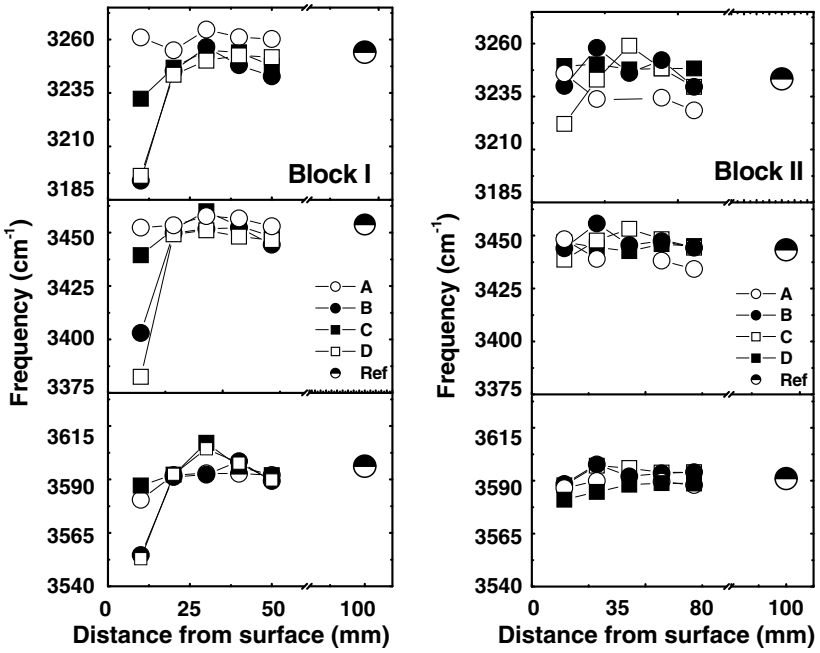


Fig. 3. Variation of stretching modes of water as a function of depth from the sodium-concrete interface for block I and block II. The half-shaded circles correspond to the values for the unexposed reference sample. Note the dramatic softening of the phonon modes in block I for samples closer to the interface.

for changes in the spectra. Heat treatment temperatures have been so chosen based on the temperature profile generated in the test blocks during sodium fire (refer Table 1) [10]. Neither the dramatic softening of modes nor the splitting of the carbonate modes of limestone observed in the sodium fire-exposed samples are evident in the heat-treated samples (Fig. 4(a)). It is clear that the spectra of the heat-treated samples did not show much of a change till about 500 °C but for a slight decrease of the sharp feature at 3643 $cm^{-1}$ due to $Ca(OH)_2$. For temperatures beyond 600 °C a dramatic increase in the $Ca(OH)_2$ feature was seen associated with a significant decrease in the overall absorption intensity of the water band (Fig. 4(b)). While the decrease in both the $Ca(OH)_2$ peak and the broad absorption due to water clearly indicate dehydration in the sample, the dramatic increase in the 3643 $cm^{-1}$ peak and the total modification of the spectra beyond 600 °C is possibly an indication of the onset of decomposition of the $CaCO_3$ aggregates first into $Ca(OH)_2$ and subsequently to calcium oxide [16]. Hence, one can now conclusively remark that the observed changes in the spectra of the sodium-exposed samples are definitely associated with the chemical interaction of hot liquid sodium with the constituents of concrete.

Table 1
Summary of test parameters and thermal parameters for both the blocks [10]

| | BlockI | BlockII |
|---|---|---|
| *Test parameters* | | |
| (a) Relative humidity open air | 77% | 63% |
| *Thermal parameters* | | |
| Peak temperature (°C) at | | |
| (a) Initial sodium dumping | 550 | 550 |
| (b) Sodium air interface | 757 | 646 |
| (c) Sodium concrete interface | 752 | 716 |
| (d) Sodium concrete interface after 5 min of dumping | 454 | 304 |
| (e) 30 mm from interface | 295 | 304 |
| (f) 110 mm from interface | 94 | 105 |

### 3.2. Reaction with fused NaOH

Further, in order to gain insight into the actual mode of attack of sodium on concrete, the reference limestone concrete samples were treated with hot fused NaOH at 450 °C, thus simulating a sodium-concrete interaction typically expected to occur [2,16] during sodium fires, and their spectrum recorded. Fig. 5 shows the spectrum of this fused NaOH treated concrete at 450 °C which is found to be similar to that of the sodium exposed sample, thus confirming the conjecture that the changes observed in the sodium degraded samples are definitely signatures of the thermochemical attack of sodium on concrete and that the mechanism of sodium attack is indeed a melt soda one. It is evident from Fig. 5 that concrete samples treated with NaOH at temperatures lower than 300 °C were unaffected. This clearly points to the fact that NaOH erodes limestone concrete only at elevated temperatures. Based on the above observations the following physical concepts of sodium-concrete interactions are found to emerge.

### 3.3. Changes in the phonon modes of water

It is well known that water in concrete is held in the following ways [2]: (a) Free water in the capillary pores, (b)

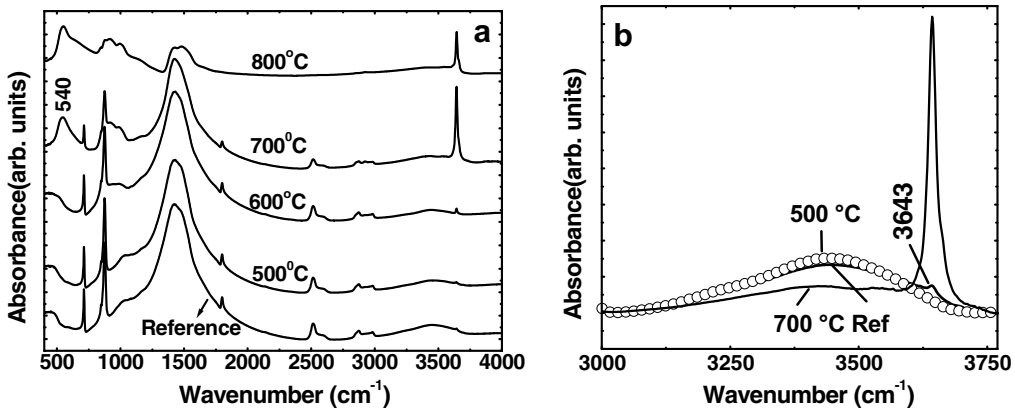


Fig. 4. (a) Infrared spectra of heat-treated reference limestone concrete samples along with the untreated sample. A dramatic increase in the 3643 $cm^{-1}$ peak is seen for temperatures beyond 600 °C. Note that for temperatures above 700 °C the spectrum gets totally modified signaling the decomposition of limestone aggregates. Right panel (b) shows the area normalised region between 3000 and 3770 $cm^{-1}$ showing the anomalous variation of the 3643 $cm^{-1}$ peak with temperature.

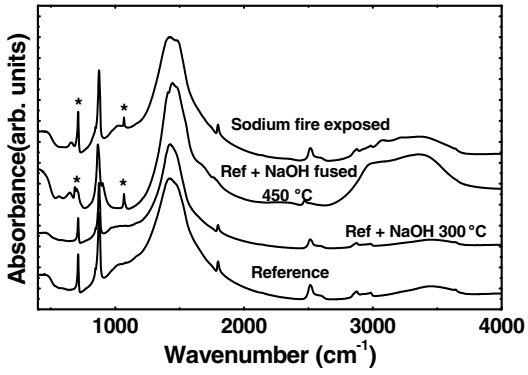


Fig. 5. Mid infrared spectra of the limestone aggregate concrete sample treated with fused NaOH (450 °C). Notice that this spectrum compares very well with the spectrum of the sodium fire-exposed sample. Spectrum of reference treated with NaOH at lower temperature is unaffected.

physically bound water in the gel pores and (c) chemically bound water in the form of hydration products.

(1) Upon contact with hot sodium at 550 °C, both free and bound water is released from inside the concrete. Direct evidence of the dehydration effects can be got by an overall decrease in the absorption intensity of water and the dramatic decrease in the 3643 $cm^{-1}$ peak due to $Ca(OH)_2$ (decomposition of the chemically bound water in the form of hydrates) (Fig. 4(b)).

(2) The water thus released is then driven to the concrete surface where it reacts with sodium through the following exothermic reaction [16].

$$Na + H_2O \rightarrow NaOH + 1/2H_2 + 38\ kcal \quad (1)$$

(3) The NaOH formed is expected to chemically erode the limestone aggregate concrete samples thus:

$$2NaOH(l) + CaCO_3(s) \rightarrow Na_2CO_3 + Ca(OH)_2 \quad (2)$$

$$Ca(OH)_2 \rightarrow CaO + H_2O \quad (3)$$

The above conversion of bound water to free water as per the above reactions would imply an increase in the extent of hydrogen bonding compared to bound water in concrete that is confined. This increased hydrogen-bonding leads to a weakening of the O–H stretch modes resulting in the observed drastic softening of modes. As mentioned earlier and as seen from Fig. 2, the sudden build-up of the low frequency hydrogen-bonded components at distances closer (20–30 mm) to the cavity surface once again suggests increased hydrogen bonding [15], thus providing additional evidence for the formation of free water. The modes of the $Na_2CO_3$/CaO formed (Eq. (2)) cannot be easily discerned since they have similar spectral features as that of $CaCO_3$ [13,17].

### 3.4. Trends in normalised area of 3643 $cm^{-1}$ peak $Ca(OH)_2$

As mentioned earlier the sharp feature at 3643 $cm^{-1}$ arises due to the major hydration product of portland cement – $Ca(OH)_2$ – and any chemical/thermal degradation in these materials is expected to decompose these hydrates and hence cause a decrease in the intensity of this peak [11]. Going by the above argument, the intensity of this mode is expected to decrease for samples removed from near the sodium-concrete interface as compared to that of the reference. The sharp peak is then expected to show a regular increase for increasing distances from the surface. While such a trend is indeed observed for block I, there seems to be absolutely no systematics followed in block II as shown in Fig. 6. Further, one can also note occasional spurts in the peak areas over and above the area of the reference sample. Based on the earlier heat treatment measurements one can infer that the 3643 $cm^{-1}$ peak is very sensitive to temperature effects – while in the initial heating regime (RT = –500 °C) this feature decreases, for still higher temperatures the peak reappears and picks up drastically (Fig. 4(b)). Hence, the observed irregular trend in the variation of the normalised peak area of

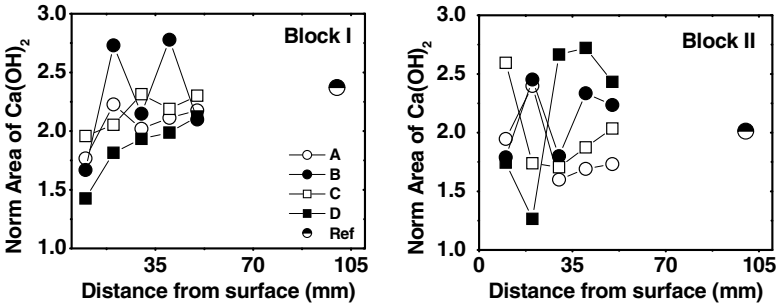


Fig. 6. Variation of the normalised area of $Ca(OH)_2$ peak at 3643 $cm^{-1}$ as a function of depth from the affected surface. Note that the variation in block I is systematic while block II exhibits a highly irregular trend. The half-shaded circles refer to the reference values plotted at 100 mm for convenience.

3643 $cm^{-1}$ peak could be a reflection/manifestation of the random movement of the thermal front in the concrete blocks possibly arising due to location wise/block wise variation in the microstructural properties of the blocks [10]. The occasional spurts in the $Ca(OH)_2$ peak intensity could be locations inside the concrete blocks where the temperatures could have momentarily exceeded 500 °C. From the above arguments and from Fig. 6 it is clear that although block I exhibits the expected increasing trend, pointing to dehydration confined to regions near the surface, block II exhibits a rather irregular variation implying random dehydration extending to the bulk.

### 3.5. Changes in the 500–3000 $cm^{-1}$ range

As earlier mentioned the limestone aggregate in the unexposed reference sample is principally in the form of calcite. It can be seen from Figs. 2 and 5 that both the sodium fire-exposed samples as well as the reference samples treated with hot fused NaOH (450 °C) show changes with respect to the appearance of a new mode at 1070 $cm^{-1}$ in addition to an evident splitting of the $\nu_2$ and $\nu_4$ modes into doublets. The new feature at 1070 $cm^{-1}$ can be identified as a Raman active $\nu_1$ mode of calcite that gets activated after interactions with hot liquid sodium. The above observations unambiguously point to a lowering of symmetry in calcite caused due to interactions with sodium possibly signaling a structural transformation of calcite [13,14]. It is to be noted here that no such signatures of a structural change is observed in the heat-treated samples even for temperatures as high as 800 °C. Hence one can now infer that the observed structural transformations are definitely associated with the chemical interactive effects of hot liquid sodium on concrete.

### 3.6. Block I versus block II

As discussed earlier and as is evident from Fig. 3, samples removed from block I show higher thermochemical degradative effects confined to the surface, while random thermal degradation seems to predominate and extend to the bulk region beneath the cavity floor for block II (Fig. 6). We have tried to relate the above behavior to various parameters recorded in the earlier report pertaining to both the blocks. (Tables 1 and 2) [10]. Although both the tests were carried out under identical conditions, the variation in test results are attributed to block wise fluctuations in both microstructural distribution of the constituents of concrete and its casting/curing conditions. Prior to sodium exposure, rebound hammer tests conducted on the cavity floors of both the concrete blocks revealed a marginally higher compressive strength and hardness for concrete block I compared to block II [10]. Hence block I would be expected to be more resistant to sodium attack compared to block II.

#### 3.6.1. Block I

The fact that the region near the cavity surface in block I has undergone marginally higher thermo-chemical degradation despite higher mechanical strength compared to block II can be correlated to the test/thermal parameters (see Table 1) recorded in the earlier study. It is indeed surprising from Table 1 that although the initial sodium dumping temperature has been the same for both blocks, the temperature recorded at the sodium air interface for block I is much higher than block II. Possible reasons for such high temperatures attained could be due to the relatively higher humidity of open air (77%) during the sodium exposure for block I that could have initiated more intense and violent reactions as compared to block II. This higher temperature has set the stage for the consistently higher temperature at regions near the interface for block I, thus, leading to a higher extent of thermochemical degradation. Further evidence of the degradation in the cavity surface can be got from the rebound hammer tests on post test concrete surfaces, which imply greater damage to the cavity

Table 2
Summary of post test mechanical parameters [10]

| Post test mechanical parameters | BlockI | BlockII |
|---|---|---|
| (a) Percentage reduction in rebound hammer test for cavity floor | 16% | 9.9% |
| (b) Extent of mass loss (% by mass) | 0.61 | 0.87 |
| (c) Percentage reduction in compressive strength | 24% | 35% |
| (d) Percentage reduction in UPV measurements | 7% | 12% |

surface of this block (Table 2). In spite of the higher temperatures attained at the interface the propagation of the thermal front into the bulk is more contained possibly due to the better quality of concrete.

*3.6.2. Block II*

Although mild effects of a chemical interaction of sodium are evident at the cavity surface, the effects are less pronounced (Fig. 3) since the temperatures recorded at the interface are much lower than the temperature recorded in block I (Table 1). On the contrary the propagation of the thermal front into the bulk is more pronounced compared to block I (Fig. 6) possibly due to its lower mechanical strength. This could imply higher levels of dehydration in the bulk (also evident from the thermal parameters in Table 1), possibly leading to greater deterioration in its mechanical strength. Ample evidence for the higher degradation in the bulk for this block has also been obtained by several post-test measurements like weight loss measurements, reduction in compressive strengths and ultrasonic pulse velocity measurements (Table 2).

## 4. Summary and conclusions

Direct evidence of the thermo-chemical degradation of limestone aggregate concrete on exposure to sodium fires have been obtained using infrared spectroscopy. Definite signatures of the conversion of bound water to free water associated with a structural modification of the limestone aggregates have been obtained as a consequence of sodium-concrete interactions. Unambiguous evidence of the exact mode of attack of sodium on concrete via the formation of NaOH has also been obtained. Although the direct reaction of NaOH with concrete is confined to the regions near the cavity surface, mild signatures of dehydration are seen to extend to the bulk. Infrared spectroscopy has thus helped to generate a depth profile of the thermo-chemical degradative effects of sodium fire on limestone aggregate concrete that could have implications on the design of a protective sacrificial layer over the structural concrete. Block wise variations observed in the degradative effects have been excellently correlated with the thermal and mechanical parameters recorded earlier (Tables 1 and 2) on both pre and post-test concrete samples which clearly point out that the intensity of damage caused to the concrete is severely influenced by the following two key factors: (a) intensity and duration of sodium fires. (b) Quality (compressive strength and hardness) of the concrete layer. Infrared spectroscopy has thus proved to be a very sensitive tool to probe the changes occurring during sodium-concrete interactions and the present work has clearly brought out the potential of this simple technique in providing a reliable and simple route to monitor this important class of reaction.

## Acknowledgements

The authors gratefully acknowledge fruitful discussions with Dr K.S. Viswanathan, Materials Chemistry Division. The authors would also like to thank Sri S. Srinivasan for his services in collecting the samples. The authors are also grateful to Sri N. Kasinathan, Head, Safety Engineering Division, for his support.

## References

[1] L.D. Muhlestein, A.K. Postma, Nucl. Safety 25 (1984) 212.
[2] G.F. Schultheiss, H.-J. Deeg, Kerntechnik 55 (1990) 274.
[3] C. Casselman, Nucl. Eng. Des. 68 (1981) 207.
[4] R.K. Hilliard, W.D. Boehmer, Concrete Protection from Sodium Spills by Intentionally Defected Liners – Small Scale tests S9 and S10, Report No: HEDL-TME 75-75 (1975).
[5] A.J. Mahncke, L.D. Muhlestein, R.W. Wiermann, R.P. Colburn, Breeder Reactor Faulted Cavity Liner Feature tests, in: Proceedings of the International Meeting on Fast Reactor Safety Technology Seattle, vol. 4, 1979, p. 2103.
[6] D.W. Jeppson, Fusion Technol. (1989) 990.
[7] H. Seino, O. Miyaki, Y. Himeno, Development of Ceramic Liner for FBR Buliding International Fast Reactor Safety Meeting, vol. 1, 1990, p. 251.
[8] H.W. Fritke, Experimental Investigation of Sodium-concrete Interactions and Mitigating Protective Layers, Transactions of the 7th International Conference of Structural Mechanics in Reactor Technology, vol. H No 3/3, 1983, p. 135.
[9] M. Bolvin, M. Mosse, B. Clatot, P. Gebergh, C. Oberlin, P. Conche, Research on concrete with acceptable Safety Characteristics Under Sodium Attack, in: Proceedings of International Conference on Science and Technology of Fast Reactor Safety, vol. 1, 1986, p. 97.
[10] F.C. Parida, S.K. Das, A.K. Sharma, P.M. Rao, S.S. Ramesh, P.A. Somayajulu, B. Malarvizhi, N. Kasinathan, in: Proceedings of the 14th International Conference On Nuclear Engineering (ICONE-14), Florida, USA, 2006.
[11] E. Fratini, Francesca Ridi, Sow-Hsin Chen, P. Baglioni, J. Phys. Condens. Mat. 18 (2006) S2467.
[12] Javed I. Bhatty, J. Dollimore, G.A. Gamlen, R.J. Mangabhai, H. Olmez, Thermochimica Acta 106 (1986) 115.
[13] M.A. Legodi, D. DeWaal, J.H. Potgeiter, Appl. Spectrosc. 55 (2001) 361.
[14] S. Gunasekaran, G. Anbalagan, Spectrochim. Acta Part A 68 (2007) 656.
[15] G.E. Walrafen, M.S. Hokmabadi, W.H. Wang, J. Chem. Phys. 85 (1986) 6964.
[16] T.C. Chawla, D.R. Pederson, Nucl. Eng. Des. 88 (1985) 85.
[17] M.J. Harris, E.K.H. Salje, J. Phys: Condens. Mat. 4 (1992) 4399.